Atomic transformation pathways from terahertz radiation generated by shock-induced phase transformations

Evan J. Reed*
Department of Materials Science and Engineering, Stanford University, Stanford, California 94304, USA
and Lawrence Livermore National Laboratory, Livermore, California 94550, USA
(Received 30 December 2009; published 26 April 2010)

This work shows that detectable terahertz (THz) frequency radiation can be emitted when a wurtzite-structure crystal transforms to a rocksalt structure under shock compression on picosecond time scales. Information about the atomic-scale transformation pathway is contained in the sign of the emitted THz electric field and information about the kinetics is contained in the time dependence. This phenomenon provides an avenue to experimental measurement of microscopic transformation pathways in crystals on the shortest (picosecond) time scales.

DOI: 10.1103/PhysRevB.81.144123 PACS number(s): 62.50.Ef, 78.55.−m

One of the far-reaching goals in current materials physics research is experimental observation of the atomic motions associated with a change in phase. Here we present a physical mechanism that can be utilized to accomplish this in some crystals lacking inversion symmetry. Observing ultrafast, picosecond time scale phase transformations and determining how they occur is extremely challenging but promises to usher in a new era of understanding and control of materials. The picosecond time scale dynamics of materials are beginning to be revealed by a cadre of innovative ultrafast x-ray, electron, and optical techniques (see, e.g., Refs. 1–3).

One of the common scenarios where picosecond time scale phase transformations occur is during shock-compression high-pressure studies, i.e., by launching a transient high-pressure wave into the material using a laser or impacting projectile (see, e.g., Refs. 4–6). Understanding high-pressure phase transformations in materials is central to planetary science and geological processes[7,8] and has been the subject of much research in CdSe for technological applications.[9–16] In this work, we show that the ultrafast, shock wave induced wurtzite to rocksalt phase transformation in CdSe is accompanied by the generation of detectable terahertz (THz) frequency electromagnetic radiation. Motion of charged ions during transformation generates electrical currents and endows the transformed material with a static electrical polarization. Remarkably, this work finds that the sign of the emitted electric field contains information about the atomic-scale transformation pathway. We demonstrate that a shift in transformation pathway with increasing shock pressure can be observed by detecting emitted THz radiation.

This work builds on recent theoretical and experimental work showing that THz frequency electrical signals are coherently generated when acoustic and shock waves propagate through ionic materials and can be utilized as a new type of ultrafast materials dynamics probe.[17–21] Motion of charged atoms in ionic materials radiates coherently when coherently excited by acoustic or shock waves. This phenomenon has recently been experimentally observed for THz frequency acoustic waves propagating through GaN/AlN heterostructures.[21] In this work, we consider an experimental scenario similar to that of Ref. 21 but at pressures sufficiently large to induce a phase transformation.

We consider CdSe rather than the GaN utilized in the experiments of Ref. 21 because CdSe exhibits a well-studied rocksalt phase transformation that occurs at relatively low pressures.[9–16] Both CdSe and GaN are piezoelectric and have the wurtzite structure. CdSe is a semiconducting material with applications in electronic and optical devices. Considerable interest has revolved around the synthesis and control of nanocrystalline forms. The wurtzite to rocksalt transformation under pressure in CdSe has been studied via experiments and molecular-dynamics simulations in the bulk[9–12] and nanocrystalline forms.[13–16] A number of different mechanisms have been proposed for the microscopic transformation pathway. In particular, simulations by Shimojo *et al.*[12] have suggested that there may be multiple competing mechanisms under hydrostatic conditions in the bulk transformation. The wurtzite to rocksalt transformation and its dynamical pathway have also been studied under the nonhydrostatic conditions of shock compression in CdS (Refs. 22 and 23) but not in CdSe.

Figure 1 schematically shows how a hypothetical one-dimensional (1D) crystal that undergoes a phase transformation can generate a static polarization. In Fig. 1(a), the top line shows a 1D chain of atoms in a wurtzitelike crystal structure (with c axis in the chain direction). Arrows show how the central atoms move to form a rocksaltlike crystal structure, i.e., equal spacing between atoms. Regions with static electric charge are created at the rocksalt-wurtzite interface. In Fig. 1(b), a different transformation mechanism results in a static polarization sign opposite to that in (a). Measurement of the sign and magnitude of the static polarization reveals the atomic transformation pathway.

Figure 2 schematically shows how polarization currents can be generated when a compression wave propagates into a wurtzite-structure material or any material that lacks inversion symmetry. Figure 2(a) shows how a compression wave generated on the left propagating to the right generates a static polarization of the compressed material due to the piezoelectric effect. The c axis of the material is oriented in the vertical direction, leading to the production of static charge on the top and bottom of the strained region. If the charge density produced is σ_1, the polarization current per unit area

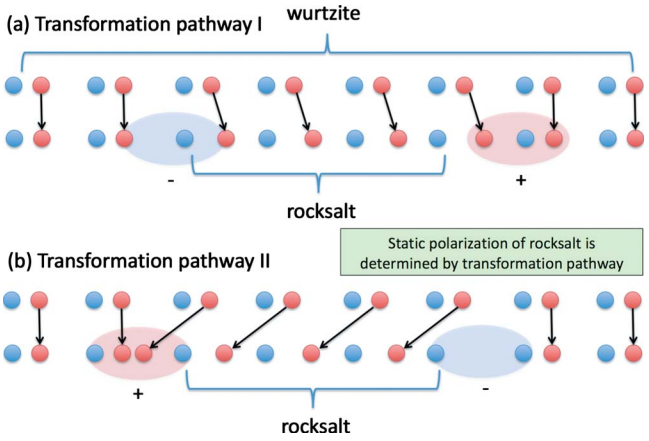

FIG. 1. (Color online) Schematic showing how a hypothetical 1D crystal that undergoes a phase transformation generates a static polarization with sign depending on the transformation pathway. (a) The top line shows a hypothetical 1D chain of atoms in a wurtzite-like crystal structure. The color denotes the electric charge. Arrows show how the central atoms can move to form a rocksaltlike crystal structure, characterized by equal spacing between atoms. Regions with static electric charge are created at the rocksalt-wurtzite interface, resulting in the formation of an electric dipole. (b) A different transformation mechanism results in a static polarization sign opposite to that in (a). Note that the rocksalt crystal is identical in both (a) and (b) cases but the sign of the electric dipole differs depending on how the atoms move to form the rocksalt. Measurement of the sign and magnitude of the static polarization reveals the atomic transformation pathway.

generated by the shock is $j=\sigma_1 v_1$ in the c lattice direction where v_1 is the propagation speed.

Figure 2(b) shows the case where the wurtzite material transforms to the rocksalt structure, accompanied by a change in static polarization. In this case the total polarization current per area is $j=\sigma_2' v_2' + \sigma_1' v_1'$. Depicted is the case where the elastic wave speed exceeds the speed of the transformation interface. Note that if σ_1' and σ_2' are of opposite signs, the polarization current j can potentially be of either sign. The polarization currents generate radiation which can be detected some distance away from the shock wave. Changes in the amplitude and/or sign of the radiation can indicate the onset of the phase transformation.

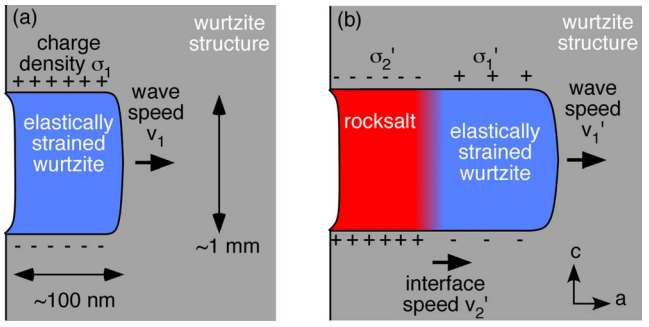

FIG. 2. (Color online) Schematic of shock waves in (piezoelectric) wurtzite generating static polarizations. (a) An elastic wave front propagates left to right with speed v_1, leaving the material behind it in a uniaxially compressed state. Static polarization charge σ_1 is generated in the c axis (vertical) direction due to the piezoelectric effect. (b) At higher pressures, a slower wave propagates behind the elastic wave. The slower wave is associated with transformation to the rocksalt structure, exhibiting a different static polarization charge $\sigma_2' \neq \sigma_1'$. Changes in amplitude and/or sign of the total polarization indicate the onset of the rocksalt transformation.

I. METHODS

To accurately explore the dynamics and fields generated by this phenomenon, we perform multimillion atom molecular-dynamics simulations utilizing the LAMMPS code[24] and the CdSe potential of Rabani[25] which consists of a Coulomb interaction (effective atomic charges of magnitude 1.18) plus a Lennard-Jones interaction. This potential has been found to reproduce the bulk wurtzite to rocksalt transition near the experimentally observed hydrostatic pressure of 2.5 GPa and the ionic nature of the representation of wurtzite and rocksalt phases has been further validated by Zahn *et al.*[11] In this work we perform nonequilibrium molecular-dynamics (NEMD) simulations of shock waves propagating down the a axis direction of CdSe single crystals. Shock experiments on single crystals are routinely performed, see, e.g., Ref. 6.

We perform shock wave NEMD simulations which are commonly employed to study shock waves in a variety of materials (see, for example, Ref. 26). Planar shock waves are generated within three-dimensional computational cells of crystalline atoms with cross section 15×15 nm^2 and length in the shock propagation direction about 200 nm. A piston consisting of rigid atoms on one side of the cell is given a constant velocity moving into the cell. A shock wave propagates away from the piston.

The electromagnetic radiation generated by the shocked material in the THz frequency regime can be calculated directly from the polarization currents per area generated in the molecular-dynamics simulation, $\vec{j}(t)=\frac{1}{A}\Sigma_i q_i \vec{v}_i(t)$, where the sum is over all atoms in the computational cell. Since CdSe is electrically insulating, we assume that electronic contributions to this spectral regime are negligible so that only the motion of the charged atoms contributes to THz polarization currents. This assumption is justified in detail in Sec. III. The electric field at a point $\vec{r}$ generated by the shocked material is calculated by assuming a point-dipole source,

$$\vec{\tilde{E}}(\vec{r},\omega)=A'\frac{\tilde{j}(\omega)}{-i\omega}\left[\left(\frac{\omega}{c}\right)^2 \hat{n}\times\hat{\epsilon}\times\hat{n} + [3\hat{n}(\hat{n}\cdot\hat{\epsilon})-\hat{\epsilon}]\left(\frac{1}{|\vec{r}|^2}+\frac{i\omega}{c|\vec{r}|}\right)\right]\frac{e^{-i(\omega/c)|\vec{r}|}}{|\vec{r}|}, \quad (1)$$

where $\vec{\tilde{j}}(\omega)=\tilde{j}(\omega)\hat{\epsilon}$ and A' is the area of the shock. The cross product term dominates in the far field and is proportional to the time derivative of the current. Static polarizations manifest themselves in the near field. In this work, a typical experimental circular shock diameter of $2\sqrt{A'/\pi}=1$ mm and distance of $|\vec{r}|=2$ mm perpendicular to the polarization dipole are considered. The field at 2 mm contains both near- and far-field components for the frequencies considered here.

The dielectric structure and geometry of the sample are neglected for simplicity here. Such details have been taken into account in earlier work.[21] We note that nearby large magnitude dielectric materials (e.g., metals) can potentially have significant impact on the efficiency of the radiative process and need to be considered for experimental work.

Since the cross-section dimensions of the computational cell are much smaller than the lateral dimension of the shock in Fig. 2, some consideration must be given to the electrostatic boundary conditions. Periodic boundary conditions maintain a periodic electrostatic potential and a zero macroscopic electric field across the computational cell. The internal macroscopic electric field in pyroelectrics is typically zero because surface charges and other defect charges screen any fields present. The generation of static charges as shown in Fig. 2 will establish a nonzero electric field in the c direction (transverse direction) that is not present in the simulation. However, the magnitude of such fields is small away from the edges of the shock. Note that the aspect ratio in Fig. 2 is exaggerated. For a circular diameter of 1 mm and $\sigma \sim 0.1$ C/m^2, the electric field near the center is on the order of $\frac{\pi\sigma}{\epsilon}\frac{d}{D} \sim 0.1-1$ kV/cm and is sufficiently small to be neglected in this geometry. The corresponding electric field cannot be neglected when the shock propagation direction is not normal to the c axis when employing periodic boundary conditions for the electrostatic interactions. In this case analogous to a parallel-plate capacitor geometry, stronger local electric fields are produced by the polarization charges.

Spectral content above 0.25 THz was filtered out of the computed polarization currents to reduce high-frequency incoherent noise. The much larger number of atoms employed in an experiment combined with the group-phase velocity mismatch of experimental electro-optic sampling THz detection techniques has a similar filtering effect.

II. RESULTS

Figure 3(a) shows the magnitude of the c (unique) axis static polarization of the material when a shock is generated by a piston speed of 600 m/s. The uniaxial strain and stress in the shock propagation direction are −0.12 and 17 GPa, respectively. The vertical axis shows distance in the shock propagation direction. The polarization of material within some region Δx in the shock propagation direction x is calculated by $P(t)=\frac{1}{A\Delta x}\int_{t_0}^{t} dt' \Sigma_{i\in\Delta x} q_i \vec{v}_i(t')\cdot\hat{z}$, where q_i and $\vec{v}_i(t)$ are the charge and velocity of atom i, A is the computational cell cross section perpendicular to x, and $\hat{z}$ points down the c axis. The initial polarization state of the wurtzite material has been arbitrarily taken to be zero in Fig. 3(a). The shock is generated by the piston at 10 ps. It propagates into the cell, inducing a positive change in static polarization due to the piezoelectric effect. The material is elastically strained from 10 to 20 ps. At 20 ps, a region of negatively polarized rocksalt begins to form near the piston and propagates away more slowly than the elastic wave. Figure 3(b) shows the coordination of the material. The material is all fourfold coordinated (wurtzite) except for the formation of sixfold coordinated rocksalt beginning around 20 ps.

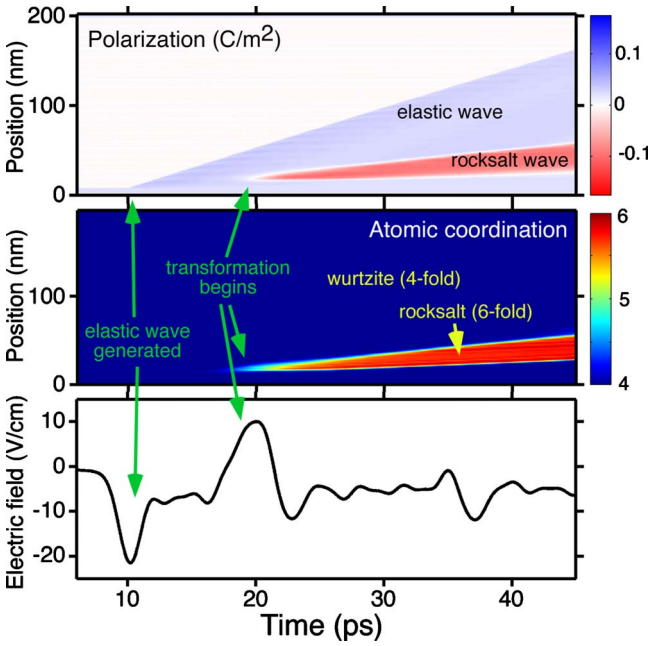

FIG. 3. (Color online) Material polarization, atomic coordination, and emitted electric field for shock generated by 600 m/s piston speed. (a) An x-t diagram for the static polarization of the material in the computational cell, showing the propagation of the elastic wave (positive polarization, blue) followed by formation of rocksalt structure (negative polarization, red) around 20 ps. (b) An x-t diagram of the atomic coordination shows the coordination of most of the material is fourfold (wurtzite) except for the rocksalt region which is sixfold coordinated. (c) The computed electric field 2 mm away shows coherent signals when the shock enters the computational cell (10 ps) and when the rocksalt transformation begins (20 ps.)

Figure 3(c) shows the time dependence of the electric field generated by the polarization currents in the simulation for a typical experimental configuration. The field is calculated 2 mm away from the shocked material where it can be experimentally detected. The peak at 10 ps corresponds to the shock entering the CdSe. Such signals were initially predicted by our earlier work[20] and subsequently experimentally observed in GaN.[21] A feature around 20 ps indicates the onset of the rocksalt phase transformation. This feature has sign opposite to the 10 ps feature because the polarization of the rocksalt material is opposite in sign to the elastically compressed wurtzite, shown in Fig. 3(a). Observation of the delay between these pulses provides information about the kinetics of the transformation.

The time dependence of the electric field from shocks of different amplitudes generated by other piston speeds is shown in the inset of Fig. 4. At 500 m/s piston speed, the phase transition begins around 30 ps, indicated by a change in slope of the field. For higher piston speeds shown, the transformation begins immediately after the shock enters the material around 10 ps as evidenced by plots of coordination and polarization. At 2 mm from the shocked material, the electric field contains both near- and far-field components. The far-field components contain the transient spikes and the near-field component grows nearly linearly with time. The

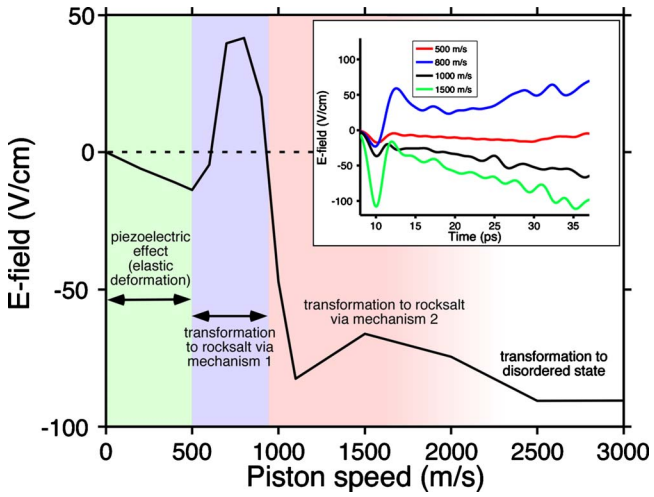

FIG. 4. (Color online) Generated electric field reveals phase transformation and shift in transformation pathway. The inset shows the time dependence of the generated electric field for a series of piston speeds or shock amplitudes. The fields are approximately described by transient components (far-field) on top of a static component (near-field) that grows with time. The larger plot shows the electric field at 25 ps for a series of piston speeds. The sign of the field reveals the sign of the static polarization of the shocked material. The onset of the wurtzite to rocksalt transformation is indicated by a flip in sign around 500 m/s. A shift in atomic transformation pathway to rocksalt is indicated by another flip in sign around 1000 m/s.

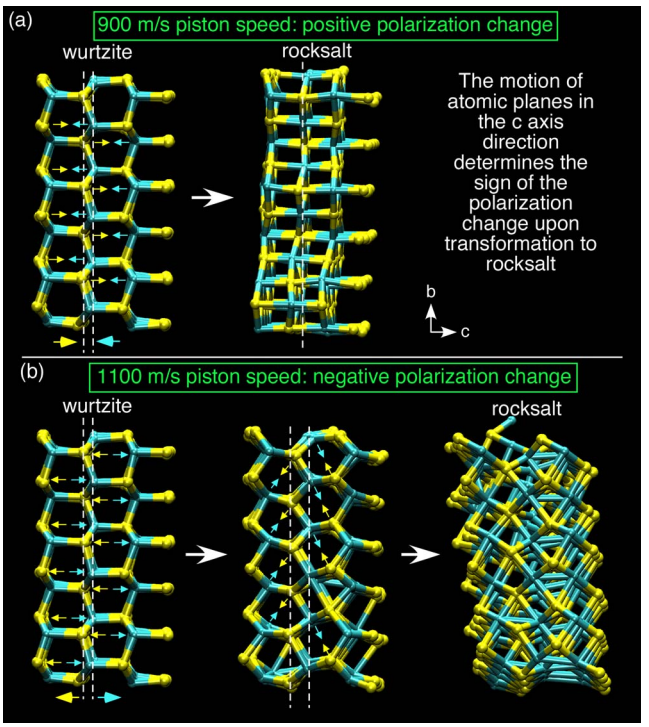

FIG. 5. (Color online) Two different wurtzite to rocksalt transformation pathways exhibit static polarizations of opposite sign. (a) Snapshots of the wurtzite to rocksalt transformation with a 900 m/s piston speed. In this case planes of Cd and Se atoms (shown by white dotted vertical lines) shift in the c direction to merge (shown by colored arrows at bottom of dotted lines.) (b) Snapshots with a 1100 m/s piston speed where a different transformation pathway is observed. In this case, planes of Cd and Se atoms move opposite in direction to the 900 m/s case, resulting in rocksalt that has polarization opposite to the 900 m/s case.

near field or static component reflects the static polarization of the material and will be the focus of the remainder of this work.

To provide a clearer picture of the field variation with shock intensity, Fig. 4 shows the electric field at 25 ps for a range of piston speeds. The field at 25 ps in all cases is largely the static component of the field, corresponding to the static polarization of the shocked material. At the lowest piston speeds, the static component has a negative sign associated with the usual piezoelectric effect: the shock strains the material which generates a static polarization. Between 500 and 1000 m/s the sign of the static field changes from negative to positive. This regime is qualitatively different from the piezoelectric regime and indicates the onset of the rocksalt phase transformation. Naively, it is not obvious how the sign should change during the wurtzite to rocksalt transformation. The sign change is determined by the atomic transformation pathway, a topic of much interest and previous work.[9–16] In this case, the sign flip makes the piezoelectric and rocksalt regimes easy to distinguish qualitatively. In the case where the sign does not change but the magnitude does, the distinction may be more challenging to interpret experimentally.

At piston speeds above 1000 m/s, the sign of the static component of the electric field in Fig. 4 becomes negative. Figure 5 shows how this sign change is associated with a change in the transformation pathway from wurtzite to the rocksalt structure. Figure 5(a) shows simulation snapshots of the transformation with a 900 m/s piston speed and Fig. 5(b) shows snapshots with a 1100 m/s piston speed, piston speeds below and above the electric field sign flip, respectively. The movement of the planes of atoms in the c axis (horizontal) direction results in changes in polarization. Such planes (basal planes) are shown by the dashed lines. In Fig. 5(a), basal planes of Cd and Se atoms move into the same plane to form rocksalt. In Fig. 5(b), basal planes of Cd and Se atoms move further apart, changing the polarization the opposite direction. Rocksalt structure is formed in both cases but differing transformation pathways lead to different resulting static polarizations of the rocksalt material.

Association of the magnitude of the static polarization with a particular transformation mechanism is complicated by the possibility of multiple transformation mechanisms at play. If multiple mechanisms are present, the polarization of the transformed material will reflect a weighted average over polarization changes in the individual mechanisms involved. To elucidate the statistical nature of the static polarization shifts, Fig. 6 shows the time dependence of the distribution of polarization of a group of 10 500 wurtzite primitive cells contained in the shocked crystal. The unit cells are located a distance 400 nm from the piston that generates the shock. The c-axis polarization of each unit cell k is determined by $p_k(t)=\int_{t_0}^{t} dt' \Sigma_{i\in k} q_i \vec{v}_i(t')\cdot\hat{z}$, where the summation over i includes all atoms in unit cell k, consisting of eight atoms. The

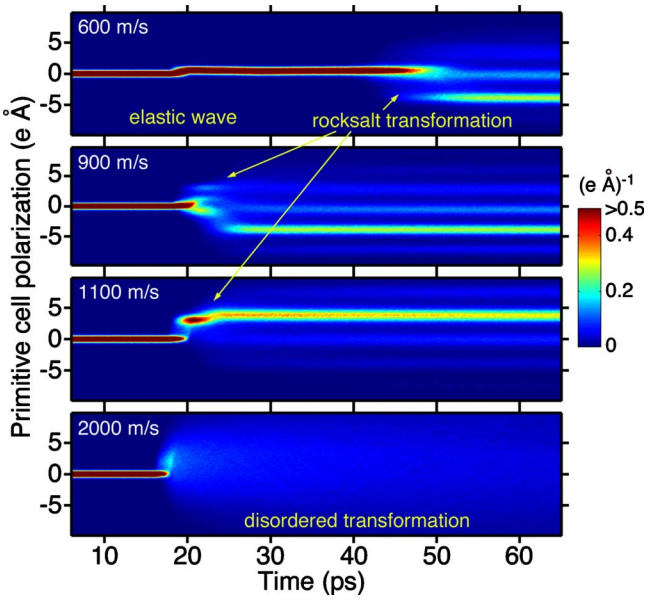

FIG. 6. (Color online) Time evolution of histogram of the polarization of wurtzite primitive cells for a series of piston speeds. These plots show that the sign of the generated electric fields in Fig. 4 reflect the sign of the polarization of most of the material, enabling identification of mechanism shifts by observing the electric field. Discretization in (a)–(c) results from crystallinity. Discretization is not observed in (d) due to disordering of the material.

distribution of unit-cell polarizations is (arbitrarily) taken to be centered around zero before the shock arrives.

Figure 6(a) shows the 600 m/s piston speed case also shown in Fig. 3. The increase in average polarization around 20 ps is associated with the arrival of the elastic wave. The changes around 50 ps occur when the slower phase transformation wave arrives. The polarization in most of the wurtzite unit cells is shifted in the negative direction, consistent with the negative average polarization of the rocksalt phase shown in Fig. 3(a). However, the polarization of some unit cells remains near zero or positive, suggesting the presence of other transformation mechanisms. Unit cells located on grain boundaries of the resulting polycrystalline rocksalt material may undergo polarization changes different from those of cells located within a rocksalt grain. The apparent discretization of the polarization values of the unit cells is associated with the crystalline nature of the transformed material.

Figure 6(b) shows the 900 m/s piston speed case. In this case, the elastic wave propagates at nearly the same speed as the phase-transition wave, both arriving around 20 ps. Like the 600 m/s case, most of the unit-cell polarizations are shifted to negative polarizations. Figure 6(c) shows the 1100 m/s piston speed case, a piston speed above the transformation mechanism shift. In this case, the polarization of most unit cells shifts in the positive direction.

Figures 6(a)–6(c) show that the polarization of most of the unit cells is correlated with the static component of the electric field in Fig. 4. Therefore, experimental observation of the static component of the field enables determination of the polarization sign shift of most of the individual unit cells.

Naively, it might be expected that a transformation to a disordered state would not be accompanied by any electric field generation since the polarization of the disordered material might be expected to be zero. Figure 6(d) shows the 2000 m/s piston speed case, where the material transforms to a disordered state. In this case, the unit-cell polarizations briefly shift up before becoming broadly and continuously distributed. Rapid diffusion of the atoms in the disordered state is indicated by a decrease in the distribution peak with time. The initial coherent shift in polarization before becoming disordered results in an observable electric field as indicated for the largest piston speed values shown in Fig. 4. The initial polarization shift suggests that the initial process of disordering occurs in a coherent fashion. Once the material is completely disordered, it is expected that the static polarization will remain constant. This form of disordering differs qualitatively from laser induced melting where atoms are observed to initially move with thermal, random velocities for the first few hundred femtoseconds.[1] In the latter case, no coherent polarization shifts would be expected during the initial stages of melting.

III. DISCUSSION

The experimental measurement of picosecond time scale solid-solid phase transformations is of considerable recent interest. The electric technique presented here provides information that is challenging or impossible to obtain with existing techniques, including x-ray diffraction. Phase transformation from bcc to hcp structures in Fe have been observed in nanosecond time scale x-ray diffraction experiments[6,27] and the atomic transformation pathway inferred from comparisons of the orientation of the resulting hcp crystals to atomic simulations.[28] The THz mechanism presented here exhibits several fundamental distinctions from such x-ray experiments. First, the THz mechanism provides information on picosecond time scales, the time scale at which many shock-induced transformations are expected to occur[4,5] and shorter time scale than the nanosecond time scale of the x-ray experiments of Ref. 28. Second, the sign of the THz contains information about the transformation mechanism that does not require atomic simulations to interpret, i.e., observation of the sign of the emitted THz is a definitive indication of a particular class of transformation pathways. Third, the THz technique potentially provides information about the transformation to a liquid state (see the sign of the liquid regime in Fig. 4). The atomic pathway for such melting transformations cannot be determined using the x-ray orientation approach of Ref. 28 because the liquid state has no orientation. X-ray and electrical techniques have a number of complimentary features that might provide the most insightful results when applied simultaneously.

This work has focused on polarization changes in the *c* direction but polarization shifts could also occur along other axes. Nonzero average polarization of the transformed material was observed only in the *b* crystalline direction in the 600 and 700 m/s piston speed cases. All other piston speeds exhibited negligible polarization shifts in the *a* and *b* crystal directions.

Considerable fundamental theoretical work on the polarization of crystals has been performed in the last few

decades.[29–31] Within the classical description of the atoms employed in this work, changes in polarization are well defined by integrating polarization currents over time. Within a quantum description of the atoms, changes in polarization of a material have been shown to be related to a geometrical Berry phase of the many-body wave function.[30] This holds when the change is adiabatic and the material remains insulating throughout the transformation. Different transformation pathways from wurtzite to the rocksalt structure manifest themselves as differing geometric phases and different static polarizations. Measurement of the resulting static polarization shift can be interpreted as a measurement of a geometric phase shift of the wave function. A perfect wurtzite crystal that transforms into a perfect rocksalt crystal will have charge density independent of the transformation mechanism but information about the transformation pathway will be contained in the wave-function phase.

Experimental observation of the sign of the static polarization of the rocksalt enables distinction between classes of transformation mechanisms but does not enable identification of a specific mechanism. For example, all of the hydrostatic wurtzite to rocksalt transformation pathways addressed by Shimojo *et al.* exhibit identical change in static polarization.[12] The observation of at least two mechanisms with opposite sign in the nonhydrostatic MD simulations here (at least one of which is unlike the mechanisms proposed by Shimojo *et al.*) indicates that the electrical measurement contains useful information. X-ray diffraction or other potentially complementary measurements are not required to make a statement about the class of transformation mechanisms observed based on the electrical measurement.

The analysis in this work assumes that electronic contributions to the polarization currents are negligible. Electronic currents flow in response to the fields generated by the static polarization shown in Fig. 2 and can potentially screen the polarization, reducing the amplitude of emitted radiation. Neglect of electronic screening is valid when the conductivities of all states of matter present in the shock and the macroscopic electric fields driving the electronic currents are sufficiently small. The electric field near the center can be shown to be on the order of $E \approx \frac{\pi\sigma}{\epsilon}\frac{d}{D}$, where $D \sim 1$ mm is the diameter of the shock, $d \sim 100$ nm is the shock propagation distance, σ is the unscreened surface charge due to the change in static polarization, and we take $\epsilon \sim 10$. For the material resistivity ρ, the time scale over which the interface charge in screened by free charge carriers is given by $\frac{\rho\epsilon}{\pi}\frac{D}{d}$. In the case of CdSe, wurtzite-structure crystals with resistivity 10^{11} Ω cm are commercially available. Assuming the resistivity of the uniaxially strained wurtzite is not significantly different, the time scale for screening is 10^3 s, well longer than the time scale of the experiment. The high-pressure rocksalt phase of CdSe has been reported to have a lower resistivity on the order of 10^{-2} Ω cm upon formation under static conditions from a single wurtzite crystal with resistivity 6×10^4 Ω cm.[32] A different resistivity value reported for the rocksalt phase formed from the zinc-blende phase is 10 Ω cm, suggesting significant variability.[32] The value of 10^{-2} Ω cm (worse case) gives rise to a screening time scale of 100 ps. While this time scale is sufficiently large to observe the effects discussed in this work, it is sufficiently small to warrant experimental consideration.

The pressure limits of the electrical effect might be expected to be determined by the increase in carrier concentration as pressure increases. Higher shock temperatures at higher pressures will lead to increased thermal carrier concentration. It is also possible that band-gap closure may occur at sufficiently high pressures or during the transformation, at which point the ionized state of the atoms ceases to exist and the analysis utilized here no longer applies. The electrical properties of CdSe undergoing the wurtzite to rocksalt transformation have been studied at the density-functional theory level by Zahn *et al.*[11] Zahn *et al.* find that the electron charges showed little variation between the wurtzite, rocksalt, and zinc-blende structures. They also studied the charges along a wurtzite to rocksalt transformation pathway and found the same result. These results suggest that the empirical approach utilized here with fixed charge values is valid at lower transition pressures.

Crystal defects are not expected to play a significant role in the electrical signals generated. While macroscopic single crystals of CdSe and other wurtzite-structure materials are commercially available and suitable for the experiments proposed in this work, some consideration of the role of defects is warranted. The total polarization of the shocked material at time t [given by $P(t) = \frac{1}{V}\int_{t_0}^{t} dt' \Sigma_i^N q_i \vec{v}_i(t') \cdot \hat{z}$] exhibits changes of order $\eta P(t)$ for a crystal defect population η. Since the defect concentration $\eta \ll 1$ for any crystal, defects have a negligible effect on the polarization currents. In fact, the rocksalt structures formed by the shock are nanocrystalline indicating that high degrees of crystallinity are not required to observe the effects in this work. However, making a meaningful statement about the atomic transformation pathway from electrical signals dictates starting with a single crystal, rather than a polycrystalline wurtzite material.

Another fashion in which crystal defects could play a role is in the kinetics of the rocksalt phase transformation in localized regions around the defect. At piston speeds of 700 m/s and above, the rocksalt phase forms as soon as the shock enters the crystal. For piston speeds below this value where the rocksalt phase forms after some nucleation time (see Fig. 3), crystal defects could play a role in kinetics of the rocksalt phase transformation as nucleation sites. Such effects will have an impact on the emitted radiation if the defect density is sufficiently high that the total volume of transformed material around all defects is greater than the untransformed material behind the shock over the homogeneous transformation induction duration (about 10 ps in Fig. 3). When the homogeneous induction time is negligible (e.g., for 700 m/s piston speeds and greater), defects are expected to play no significant role in the polarization currents for any $\eta \ll 1$.

Experimental observation of this phenomenon has a number of challenges but is likely to be possible with existing technology. THz emission on the order of 1 V/cm has been observed from elastic waves propagating through (piezoelectric) GaN structures by averaging over many shots to improve the signal-to-noise ratio.[21] The latter experiment is a lower shock amplitude variation in the experiment discussed in this work. The distinguishing challenge of the CdSe phase transformation experiment is the destructive nature of the experiment. The sample is irreversibly altered during each

shot, preventing repetitive experiments from being performed at the same place on the sample. A sample rastering scheme must be utilized. The electric fields that are generated are expected to be in the 10–100 V/cm range several millimeters from the shocked material. Shocks of the amplitudes considered in this work are routinely generated using table-top scale and larger lasers.

While the experiments of Ref. 21 are the most closely related to those proposed in this work, a number of other experimental efforts are also related. At sufficiently high shock pressures to induce a phase transformation, large amplitude microsecond time scale voltage spikes have been experimentally observed in ferroelectric materials.[33] The present work considers much faster time scales (picoseconds versus microseconds) and shows that information about the atomic transformation pathway is contained in the emitted THz signals. Some further experimental evidence exists for other forms of electromagnetic radiation that are correlated with acoustic or shock wave processes.[34,35] THz signals have been previously observed from a wide variety of ultrafast charge-transfer processes[36] and more recently from the coherent motion of charged protons in biomolecular systems.[37]

ACKNOWLEDGMENTS

The author is grateful for helpful conversations with Michael Armstrong, Aaron Lindenberg, Richard Martin, and Babak Sadiqh. This work was supported by the LLNL LDRD program and performed in part under the auspices of the U.S. Department of Energy by Lawrence Livermore National Laboratory under Contract No. DE-AC52-07NA27344.

*evanreed@stanford.edu

[1] A. M. Lindenberg, J. Larsson, K. Sokolowski-Tinten, K. J. Gaffney, C. Blome, O. Synnergren, J. Sheppard, C. Caleman, and A. G. MacPhee, Science **308**, 392 (2005).
[2] N. Gedik, D.-S. Yang, G. Logvenov, I. Bozovic, and A. H. Zewail, Science **316**, 425 (2007).
[3] C. Guo, G. Rodriguez, A. Lobad, and A. J. Taylor, Phys. Rev. Lett. **84**, 4493 (2000).
[4] D. H. Robertson, D. W. Brenner, and C. T. White, Phys. Rev. Lett. **67**, 3132 (1991).
[5] K. Kadau, T. C. Germann, P. S. Lomdahl, and B. L. Holian, Phys. Rev. B **72**, 064120 (2005).
[6] D. H. Kalantar, J. F. Belak, G. W. Collins, J. D. Colvin, H. M. Davies, J. H. Eggert, T. C. Germann, J. Hawreliak, B. L. Holian, K. Kadau, P. S. Lomdahl, H. E. Lorenzana, M. A. Meyers, K. Rosolankova, M. S. Schneider, J. Sheppard, J. S. Stolken, and J. S. Wark, Phys. Rev. Lett. **95**, 075502 (2005).
[7] S. H. Kirby, W. B. Durham, and L. A. Stern, Science **252**, 216 (1991).
[8] R. J. Hemley, *Ultrahigh-Pressure Mineralogy: Physics and Chemistry of the Earth's Deep Interior* (Mineralogical Society of America, Washington, DC, 1998).
[9] H. Sowa, Acta Crystallogr., Sect. A: Found. Crystallogr. **57**, 176 (2001).
[10] M. Wilson and P. A. Madden, J. Phys.: Condens. Matter **14**, 4629 (2002).
[11] D. Zahn, Y. Grin, and S. Leoni, Phys. Rev. B **72**, 064110 (2005).
[12] F. Shimojo, S. Kodiyalam, I. Ebbsjo, R. K. Kalia, A. Nakano, and P. Vashishta, Phys. Rev. B **70**, 184111 (2004).
[13] S. H. Tolbert and A. P. Alivisatos, J. Chem. Phys. **102**, 4642 (1995).
[14] J. N. Wickham, A. B. Herhold, and A. P. Alivisatos, Phys. Rev. Lett. **84**, 923 (2000).
[15] K. Jacobs, D. Zaziski, E. C. Scher, A. B. Herhold, and A. P. Alivisatos, Science **293**, 1803 (2001).
[16] M. Grünwald, E. Rabani, and C. Dellago, Phys. Rev. Lett. **96**, 255701 (2006).
[17] E. J. Reed, M. Soljačić, R. Gee, and J. D. Joannopoulos, Phys. Rev. Lett. **96**, 013904 (2006).
[18] E. J. Reed, M. Soljacic, R. Gee, and J. D. Joannopoulos, Phys. Rev. B **75**, 174302 (2007).
[19] E. J. Reed, M. Soljacic, and J. D. Joannopoulos, Phys. Rev. E **75**, 056611 (2007).
[20] E. J. Reed, M. R. Armstrong, K. Y. Kim, and J. H. Glownia, Phys. Rev. Lett. **101**, 014302 (2008).
[21] M. R. Armstrong, E. J. Reed, K.-Y. Kim, J. H. Glownia, W. M. Howard, E. L. Piner, and J. C. Roberts, Nat. Phys. **5**, 285 (2009).
[22] S. M. Sharma and Y. M. Gupta, Phys. Rev. B **58**, 5964 (1998).
[23] M. D. Knudson, Y. M. Gupta, and A. B. Kunz, Phys. Rev. B **59**, 11704 (1999).
[24] S. J. Plimpton, J. Comput. Phys. **117**, 1 (1995).
[25] E. Rabani, J. Chem. Phys. **116**, 258 (2002).
[26] A. Strachan, A. C. T. van Duin, D. Chakraborty, S. Dasgupta, and W. A. Goddard, Phys. Rev. Lett. **91**, 098301 (2003).
[27] B. Yaakobi, T. R. Boehly, D. D. Meyerhofer, T. J. B. Collins, B. A. Remington, P. G. Allen, S. M. Pollaine, H. E. Lorenzana, and J. H. Eggert, Phys. Rev. Lett. **95**, 075501 (2005).
[28] J. Hawreliak, J. D. Colvin, J. H. Eggert, D. H. Kalantar, H. E. Lorenzana, J. S. Stolken, H. M. Davies, T. C. Germann, B. L. Holian, K. Kadau, P. S. Lomdahl, A. Higginbotham, K. Rosolankova, J. Sheppard, and J. S. Wark, Phys. Rev. B **74**, 184107 (2006).
[29] R. M. Martin, Phys. Rev. B **5**, 1607 (1972).
[30] R. D. King-Smith and D. Vanderbilt, Phys. Rev. B **47**, 1651 (1993).
[31] R. Resta, Rev. Mod. Phys. **66**, 899 (1994).
[32] A. Onodera, Rev. Phys. Chem. Jpn. **39**, 65 (1968).
[33] S. I. Shkuratov, E. F. Talantsev, L. Menon, H. Temkin, J. Baird, and L. L. Altgilbers, Rev. Sci. Instrum. **75**, 2766 (2004).
[34] B. Hayes, J. Appl. Phys. **38**, 507 (1967).
[35] C. J. Stanton, G. D. Sanders, R. Liu, G. W. Chern, C. K. Sun, J. S. Yahng, Y. D. Jho, J. Y. Sohn, E. Oh, and D. S. Kim, Superlattices Microstruct. **34**, 525 (2003).
[36] C. A. Schmuttenmaer, Chem. Rev. **104**, 1759 (2004).
[37] G. I. Groma, J. Hebling, I. Z. Kozma, G. Varo, J. Hauer, J. Kuhl, and E. Riedle, Proc. Natl. Acad. Sci. U.S.A. **105**, 6888 (2008).